# Modified iterative learning controller for efficient power management of hybrid AC/DC microgrid

S. Angalaeswari and K. Jamuna*

School of Electrical Engineering,
Vellore Institute of Technology,
Vanadlur-Kelambakkam Road,
Chennai-600127, Tamilnadu, India
Email: angalaeswari.s@vit.ac.in
Email: jamuna.k@vit.ac.in
*Corresponding author

**Abstract:** In this paper, modified ILC is proposed for maintaining stable voltage, frequency and for efficient power management in a hybrid micro grid (HMG). The system is modelled with solar, battery, DC loads at DC bus, wind turbine, utility grid and AC loads at AC bus. An interlinking converter (IC) is connected between the AC and DC bus to facilitate bidirectional power flow. The control of voltage at AC/DC bus and management of power are obtained in the modelled hybrid micro grid with set point weighting iterative learning controller (SPW-ILC) by controlling the interlinking converter both in autonomous and grid connected mode of operation. To minimise the error signal to the controller, the classical optimisation method of sequential quadratic programming (SQP) has been employed to improve the performance of the controller. The simulation results show that the proposed controller have better performance than other controllers under variable source and load conditions.

**Keywords:** iterative learning controller; ILC; hybrid microgrid; HMG; power management; sequential quadratic programming; SQP; voltage stability.

**Reference** to this paper should be made as follows: Angalaeswari, S. and Jamuna, K. (2021) 'Modified iterative learning controller for efficient power management of hybrid AC/DC microgrid', *Int. J. Innovative Computing and Applications*, Vol. 12, No. 1, pp.24–36.

**Biographical notes:** S. Angalaeswari received her BE in Electrical and Electronics Engineering from Alagappa Chettiar College of Engineering and Technology, Karaikudi, Tamilnadu, India in 2002. She has completed her ME in Power Systems Engineering with gold medal from College of Engineering, Anna University, Chennai, Tamilnadu, India in 2009. Currently, she is working as an Assistant Professor at the School of Electrical Engineering, Vellore Institute of Technology (VIT) Chennai Campus, India from 2014. Her research areas include optimal power flow in microgrid, optimisation algorithm implementation in microgrid and controller design for hybrid microgrids.

K. Jamuna is an Associate Professor at the School of Electrical Engineering, VIT Chennai. She has 15+ years of teaching experience in various engineering colleges. She received her PhD at IIT Madras in the area of power system, her Master in Power Systems Engineering from College of Engineering Trivandrum, India and her Bachelor in Electrical and Electronics Engineering from Thiagarajar College of Engineering, Madurai, India. Her research interests are smart grid, power system state estimation, wide area measurement systems and control. She has published many papers in international journals and conferences.

## 1 Introduction

The distribution side management faces many challenges in reliability and maintenance because of the increment in the electricity demand (Mengelkamp et al., 2018). Distributed generation (DG) system has introduced to overcome these kinds of challenges. In DGs, the power generation units are placed near to the load centres (Marzband et al., 2017; Angalaeswari and Jamuna, 2015). The irregular and unreliable features of the distributed energy resources (DERs) could reason unpredictable issues when linking to the utility grid or functioning autonomously. Hence, the microgrid idea is suggested which has distributed generators and loads connected to distribution grid through point of common coupling (PCC) (Moradi et al., 2016). Microgrids are the small scale generation units that can function in an autonomous way or along with the macro grids. Microgrids contain numerous generation units comprising both renewable energy sources (RESs) and conventional energy resources (Liu et al., 2016). However, during the integration of these sources, some issues such as power loss, reduction in voltage quality and inefficient operation of generation units can be occurred.

The attention towards the microgrid is high due to its efficient and flexible operation. It may plug-in or else plug-out from the main grid that represents, it could function either beneath a grid-connected or an autonomous scheme (Chuang et al., 2016). Meanwhile, the AC power system has been existent for a long period, and collective loads are essentially AC types. Usually, the microgrid is similar to the AC microgrid (Yang et al., 2018). Nonetheless, a tendency for linking DC loads besides AC power systems is developing to conserve energy and reduce carbon contents that need a numerous quantity of inverters to transform from DC power to AC power in an AC microgrid. For specific DC generations units, the DC-to-DC converters are crucial to control the DC output to the DC bus equivalent level. Multi-level transformations can lead to power loss and degrade the power quality. Hence, the hybrid microgrid (HMG) idea is suggested to overcome the faults produced by AC or else DC microgrids (Xia et al., 2017).

A HMG comprises both AC and DC bus along with AC and DC loads. It integrates the benefits of the AC as well as DC microgrids and similarly evades their drawbacks that make it real-world in utilisation and a probable circulation form in future (Sun et al., 2017). The DC sub-grid can be deliberated as a distinctive power production unit that coupled to an AC bus through an interlinking inverter (Allam et al., 2018). As the HMG delivers a solution for the DG system, analysis on the several phases of the hybrid AC/DC microgrid has been incorporated (Li et al., 2018).

In recent times, the utilisation of distributed control in microgrids has been an interesting area because of the aforementioned benefits compared with centralised control systems. Suitable controllers such as primary, secondary and tertiary controllers are designed in DC microgrid to manage the proper load sharing (Moayedi and Davoudi, 2016). The technologically advanced controller performance is far along enhanced to deliberate the influences of communication latency (Lai et al., 2016), undefined communication structure and communication link outages and parameter improbabilities (Lu et al., 2017). Communication based distributed control arrangements for energy storage systems (ESS) is established in certain modern collected works (Lai et al., 2016) to attain specific objectives like balancing battery state-of-charge (SOC) and energy. A distributed cooperative controller based on SOC was advanced to decrease voltage swelling in the distribution feeder because of high penetration of photo voltaic (PV) systems (Morstyn et al., 2018; Zeraati et al., 2018; Mahmud et al., 2017).

For PV-battery based 1-$\phi$ autonomous microgrid, distributed consensus procedure is preferred (Golsorkhi et al., 2017). However, no studies are deliberated for simultaneous voltage regulation of an AC in addition to DC bus that a crucial necessity, mostly for a standalone hybrid AC/DC microgrid. Furthermore, efficient utilisation of battery storage in a microgrid across appropriate coordination needs supplementary research. In addition, many of the investigation focus on examining the functioning in a stable operation mode. The microgrid execution throughout mode switching is correspondingly significant as the microgrid is liable for the voltage as well as frequency regulation exclusive of utility grid support, and consequently the transient instances beneath the standalone approach of a microgrid scheme (Liu et al., 2018).

Moreover, the power generation from RESs is not a constant one. These sources are mainly dependent on the atmospheric conditions like sun irradiation, outside temperature, and speed of the wind, etc. To overcome the concerns about the variable sources, hybrid wind-solar systems are mostly used. However, solar cannot generate power during the night and wind is not blowing throughout the year. In these situations, battery energy storage systems (BESS) are used to deliver power to the load. Hence, to provide an effective, coordinated control between the AC and DC microgrid, the controller optimisation is more essential. This article presents a novel set point weighting iterative learning controller (SPW-ILC) to provide better power management in the hybrid AC/DC microgrid systems. A sequential quadratic programming (SQP) technique has been introduced to optimise the parameters of the proposed iterative learning controller (ILC). The suggested controller has been tested with different working environments, i.e., change in load, changes in source, grid-connected, and standalone modes and provides better reliability in the hybrid AC/DC microgrid system.

The novelties of the proposed work are as follows:

- development of novel SPW-ILC to enhance the performance of conventional ILC
- stability analyses of ILC (proposed SPW-ILC) with forgetting factor and with low pass filter circuit
- implementation of proposed SPW-ILC controller for IC in HMG to optimise power sharing, maintain voltage and frequency stability under input solar insolation variation and time-varying loads in both autonomous and grid connected modes of operation
- minimisation of the error signal to the controller using SQP algorithm.

The major contribution in this paper is the implementation of novel SPW-ILC which is a type of repetitive controller that can be used for doing repetitive tasks. The stability analysis of ILC for both forgetting factor and low pass filter circuits have been analysed and presented in the paper. In order to illustrate the variable input and load conditions, the simulation is being carried out in different cases under autonomous and grid connected mode of operation.

The organisation of this paper is follows as: Section 2 comprises modelling of HMG; Section 3 describes the proposed methodology. Section 4 describes the results and discussion followed by the conclusion and future work in Section 5.

## 2 Modelling of microgrid

The HMG scheme is demonstrated by incorporating dc and ac sub-grids. The architecture of the proposed scheme is illustrated in Figure 1. In the proposed microgrid, the dc bus voltage is maintained at 415 V at the output of every source present in the system.

**Figure 1** HMG system structure

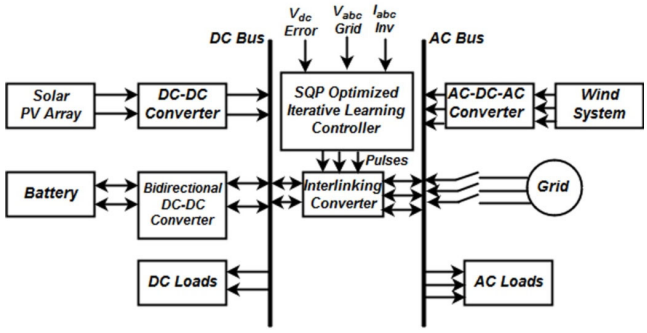


The power rating of the PV system is regulated to deliver about 7 kW, and a devoted controller controls PV system in the DC microgrid. Furthermore, a battery is connected with the bidirectional dc-dc converter to store the power during the excessive power generation and supplies power to the grid when the load requirement is increased. In the AC microgrid, a 3 kW wind turbine is connected with the AC-DC-AC converter to obtain a controllable power. Furthermore, in the AC microgrid side, the utility grid is connected with the breaker. The breaker is used to choose the operation of the HMGs in the grid connected and standalone mode of operation. Both the DC and AC microgrid are interconnected with the bidirectional converter. The modelling of power sources is explained in the following section.

### *2.1 Solar power system modelling*

The solar cell is made by uniting p and n-type semiconductor material in a thin layer. The solar cell transforms solar energy into electrical energy. In the meantime, they accurately produce less voltage in a larger current density. Consequently, a solar cell demonstrates current source nature. For determining the behaviour of the solar cell, numerous equivalent circuit arrangements exist in the literature (Deihimi et al., 2016). Normally, one diode equivalent circuit is mostly used. Figure 2 shows the electrical equivalent circuit of crystalline silicon solar.

**Figure 2** Equivalent circuit of solar cell

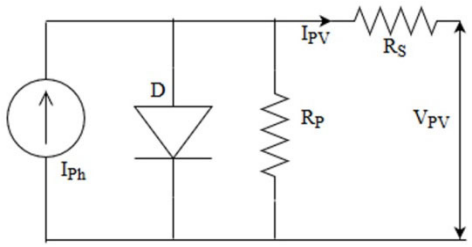


The mathematical correlation between the solar cell and current-voltage can be stated with (1), by utilising the semiconductor theory. The equivalent circuit current is

$$I_{Ph} - I_o\left(\exp\left(\frac{V_i}{nV_T}\right) - 1\right) \tag{1}$$

$$V_T = \frac{N_S kT}{q} \tag{2}$$

In real solar panels, the current-voltage characteristics cannot be established by utilising only (1). The correlation concerning the solar panel outputs current is conveyed by (1) through making an allowance for the losses presented as a resistor in Figure 2.

$$I_{PV} = I_{Ph} - I_o\left(\exp\left(\frac{V_{PV} + I_{PV}R_S}{nV_T}\right) - 1\right) - \frac{V_{PV} + I_{PV}R_S}{R_P} \tag{3}$$

The current-voltage characteristics are dependent on the quantity of solar panels utilisation. When the irradiation is rising, the current and power values gotten from solar panel are also rising. Likewise, these values are reduced based on the reduction in irradiation level.

### *2.2 Wind energy conversion system modelling*

Wind turbines utilise the kinetic energy of wind dependent on the blades swept area. The kinetic energy reasons rotation is specified in (4).

$$E = \frac{1}{2}\rho_A v V^2 \tag{4}$$

When the blade swept area is $A_T$ and wind velocity is V, the theoretical power can be obtained from the wind and is calculated by (5).

$$P = \frac{1}{2}\rho A_T V^3 (W) \tag{5}$$

From equation (5), the power generated from wind turbine is based on blade area and wind speed. Though these constraints affect the power attained from the wind scale, the significant constraint is the wind speed. These theoretic computations specify a remote scheme exclusive of any exterior issues. The maximum power acquired from a wind turbine be contingent on turbine efficiencies ($C_p$), gear mechanism efficiency, mechanical coupling efficiency in addition to generator efficiency. $C_p$ is defined as the quantity of energy transformed from wind energy to electricity and computed by

$$C_P = \frac{P_r}{P_w} \tag{6}$$

The power equation that positioned before the turbine blades are computed by

$$P_m = \frac{1}{2}\rho\frac{16}{27}AV^3(W) \tag{7}$$

16/27 = 0.593 is specified as Betz Limit at (7), and it is stated that the turbine cannot get greater than 59.3% of wind power. According to the clarifications stated beyond, the power that can be achieved from a wind turbine can be stated as.

$$P_m = C_P\left(\frac{1}{2}\rho A V^3\right)(W) \tag{8}$$

### *2.3 Battery*

For storing electrical energy, the BESS is utilised in small scale RES. The energy usage of solar power, and wind power is temporal and non-compliance. Like this, the energy continuousness of independent loads is delivered in the energy-generating schemes as per the atmospheric situations, day/night and seasonal variations. Storing the power in non-conventional energy schemes, mainly appropriate amount/performance relation and extraordinary atmosphere results concerning recycling are provided by means of lead-acid batteries.

The mathematical modelling of BESS comprises two RC circuits linked in series, an open-circuit voltage ($V_{oc}$) and an internal resistance ($R_a$) as shown in Figure 3.

**Figure 3** Equivalent circuit of battery

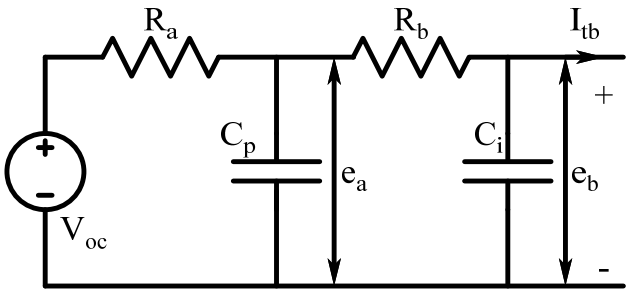


**Figure 4** Control circuit of battery

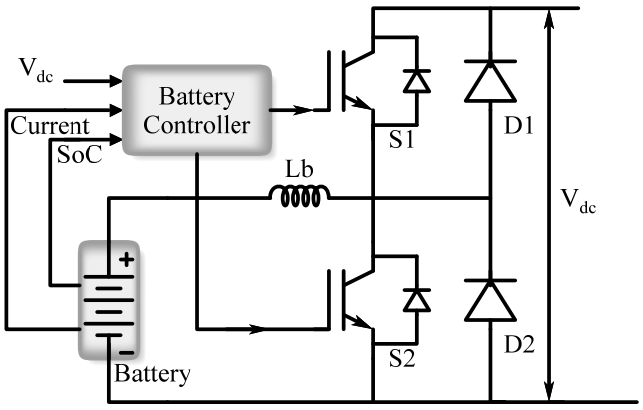


The efficient HMG's power management is achieved by maintaining the bus voltages and attain the proper power sharing among the input renewables which could be achieved by control the storage devices in all modes and controlling the interlinking converter's output in grid connected mode. The dc bus voltage along with the battery current and SoC are taken as the control variables for the battery controller as shown in Figure 4.

These constraints are the functions of the battery SOC. The $e_a$, $e_b$, and SOC are state variables and it can be computed as follows (Sedaghati and Shakarami, 2019):

$$V_{OC} = 338.8*[0.94246 + 0.05754*SOC] \tag{9}$$

$$R_a \cdot C_p \cdot \frac{de_a}{dt} + \frac{(R_a + R_b)}{R_a} \cdot e_a = V_{OC}\frac{R_a}{R_b}e_b \tag{10}$$

$$R_b \cdot C_i \cdot \frac{de_b}{dt} + e_b = e_a - R_b \cdot I_{tb} \tag{11}$$

$$\frac{dSOC}{dt} = \frac{I_t}{Q_m} \tag{12}$$

The battery current ($I_{tb}$) can be computed as:

$$I_{tb} = \frac{\left[V_{oc} - \sqrt{V_{oc}^2 - 4(R_a + R_b)P_b}\right]}{2(R_a + R_b)} \tag{13}$$

## 3 SQP optimised ILC

In the proposed system, a SQP technique is utilised to optimise the controller parameters of the hybrid AC/DC microgrid.

### *3.1 Sequential quadratic programming*

SQP technique is one of the best methodologies for solving nonlinearly constrained optimisation issues. This applied technique which develops among many specific algorithms is appropriate for small and enormous issues, and it is all around coordinated for solving substantial nonlinearities problems. SQP method permits to direct assumption of Newton's technique for constrained optimisation. At numerous emphases, this approximation is constructed from the Hessian of the Lagrangian function through a quasi-Newton updating technique (Kim et al., 2018). Since SQP technique iteratively works out successive of quadratic sub problems, it is called as recursive quadratic programming (QP) or iterative QP. A SQP technique is most efficient method to find solutions for the power system related problems in faster and effective control compared to other optimisation techniques.

However, the general SQP technique which is used for minimising or maximising the objective function is defined as:

$$Minimise\ r(y) \tag{14}$$

Subject to:

$$h_i(y) = 0 \quad i = 1,\ldots\ldots,n_e \tag{15}$$

$$g_i(y) \le 0 \quad i = n_e + 1,\ldots,n \tag{16}$$

where

$$r : S^m \to S,\ h : S^m \to S^{ne},\ g : S^m \to S^n.$$

'*h*' and '*g*' – Constraint functions estimated at '*y*',

'*r*' – linear of a quadratic objective function, '*y*' – vector, '*m*' – length.

The SQP technique substitutes the objective function '*r*' by the quadratic approximation of the Lagrangian function.

$$L(y,\lambda) = r(y) + \sum_{i=1}^{ne} \lambda_i \cdot h_i(y) + \sum_{i=1}^{n} \sigma_i \cdot g_i(y) \tag{17}$$

Assume that the bound restraints have been communicated as a disparity requirement. The QP sub-problem by nonlinear restraint linearisation is acquired as (Pavlos 2009).

$$Min \frac{1}{2} e^T H_k e + \nabla r(y_k)^T \cdot e \qquad e \in S^m \tag{18}$$

$$\nabla h_i(y_k)^T \cdot e + h_i(y_k) = 0 \qquad i = 1,\ldots\ldots n_e. \tag{19}$$

$$\nabla g_i(y_k)^T \cdot e + g_i(y_k) \le 0 \qquad i = n_e + 1,\ldots\ldots n. \tag{20}$$

At this level, the QP algorithm is utilised to take care of this sub-problem. Here three principal stages are used to execute SQP strategy, the primary stage is an updating of Hessian network followed by QP arrangement lastly by line search and merit function. In this paper, SQP has been implemented to optimise the controller inputs; to minimise the error to the controller. In order to maintain the bus voltages, DC link voltage is being compared with the reference voltage and the error is given to the ILC after SQP optimisation. The inequality constraints considered are the voltage limits, real power generation limits and the equality constraints as power balance equation. Though SQP is sensitive to the starting point selection for other optimisation problems which may lead to settling at local optima, SQP have high efficiency than other methods. Hence SQP is chosen for the minimisation of error of the controller input effectively.

The problem statement has been formulated as

$$Minimise \int E_{dcbus} \tag{21}$$

where $E_{dcbus} = V_{dcref} - V_{dcbus}$ is the error between the reference (415V) and the actual value.

Subject to

$$P_{DG\min} \le P_{DG} \le P_{DG\max}; V_{\min} \le V_{dc} \le V_{\max}; \tag{22}$$

$$P_{DG} + P_{UG} = P_L + P_{Loss} \pm P_b; \tag{23}$$

where $P_{DG}$ is the power output from the *DG* in *W*; $P_{DG\min}$ and $P_{DG\max}$ are its minimum and maximum limits; $V_{dc}$ is the dc bus voltage in *V*; $V_{\min}$ and $V_{max}$ are its minimum and maximum limits; $P_{UG}$ is the power from the utility grid; $P_L$ is the total load in the system in *W*; $P_{Loss}$ is the loss in the system and $P_b$ is the power from the battery which depends on the charging and discharging mode.

### *3.2 Iterative learning controller*

ILC is a type of repetitive controller that takes the reference and disturbance parameters repetitively either implicitly or explicitly to reduce the control errors. Since ILC is more versatile and used for continuous/discrete type of control action, it has been adopted widely in many applications. ILC is being considered as an effective control method for improving the transient response of any system having repetitive action by incorporating the information about the error obtained from the previous iteration into control for next iterations. Hence, high performance can be achieved with low tracking error in any systems under uncertain and disturbing conditions. ILC has been patented for actuator's control in US by Garden in 1971 and it has applied to the academic field in 1978 by Uchiyama.

Arimoto et al. (1990) named the ILC in 1984 which is applied for industrial driving applications especially for voltage control of the DC servo motor. The utilisation of ILC twigs from robotics industry for repetitive actions. ILC has been considered as an intelligent control method to overcome the drawbacks of the conventional controller for obtaining the desired transient response. The general ILC learning rule is in the form of equation (24) and its structure is shown in Figure 5(a).

$$u_{i+1}(z) = u_i(z) + k\varnothing(z)e_i(z) \tag{24}$$

**Figure 5** (a) Structure of ILC (b) With forgetting factor

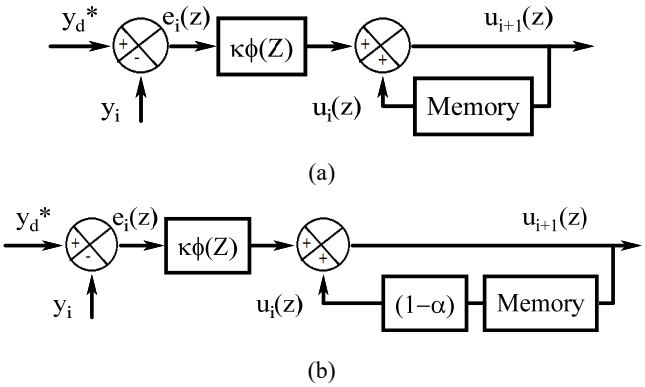


The equation (24) is employed in direct proportional ILC (P-ILC) for control action by knowing the present error and past command signal. The inclusion of forgetting factor in the ILC shown in Figure 5(b) increases the controller robustness under the noise, initialisation error and system dynamics (Deng et al., 2007) and it is expressed in (25):

$$u_{i+1}(z) = (1-\alpha)u_i(z) + k\Phi(z)e_i(z) \tag{25}$$

To prevent the over learning of the controller, the equation (25) can be realised with a low pass filter as follows (Ufnalski et al., 2018) and its structure is shown in Figure 6.

$$u_{i+1}(z) = Q_{LPF}u_i(z) + K_{RC}e_i(z) \tag{26}$$

The selection of forgetting factor or low pass filter depends on the application. In this paper, the ILC has been implemented in both the way and the stability of the system in two cases has been analysed. In first case, the forgetting factor ILC has been considered with the value of 0.04 (optimum value has obtained from the range of (0.005-0.05). The system transfer function with the input of error signal E(s) and the output of U(s) for the proposed

forgetting factor ILC has been evaluated as (27)

$$\frac{U(s)}{E(s)} = \frac{0.0009819s + 4.77e^{-5}}{s^2 + 0.0724s + 0.0006303} \tag{27}$$

Poles for the system have been determined as –0.0623 and –0.0101. The system is completely stable with the transfer function.

**Figure 6** ILC realised with forgetting factor or low pass filter

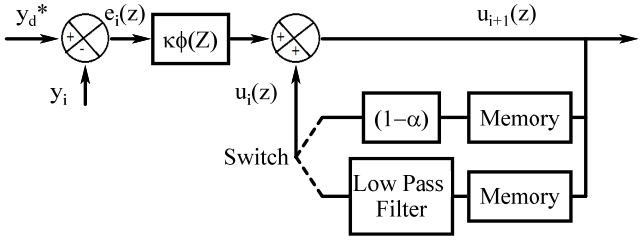


The system transfer function with low pass filter ILC with filter function of $Q(z) = \frac{0.25 + 0.5z^{-1} + 0.25z^{-2}}{1}$ (Ufnalski et al., 2018) has been evaluated as (28)

$$\frac{U(s)}{E(s)} = \frac{0.0007876s - 1.991e^{-7}}{s^2 + 0.0001934s + 1.606e^{-8}} \tag{28}$$

Poles for the system have been determined as

$$1e^{-4}\begin{bmatrix} -0.967 + 0.8191i \\ -0.967 - 0.8191i \end{bmatrix}.$$

The poles of the system with forgetting factor are more stable than the controller with filter.

### *3.3 Set point weighting ILC*

In Direct P type ILC, the introduction of forgetting factor $\alpha$ provides stable and required tracking ability for the controller. In order to improve the performance of the ILC, modified ILC has been proposed in this paper by introducing the set point weighting factor $\beta$ with the range of (0–1) as in (29):

$$u_{i+1}(z) = \beta\left(1 - \sqrt{\alpha}\right)u_i(z) + K_{RC}e_i(z) \tag{29}$$

**Figure 7** Selection of optimum value of $\alpha$ (see online version for colours)

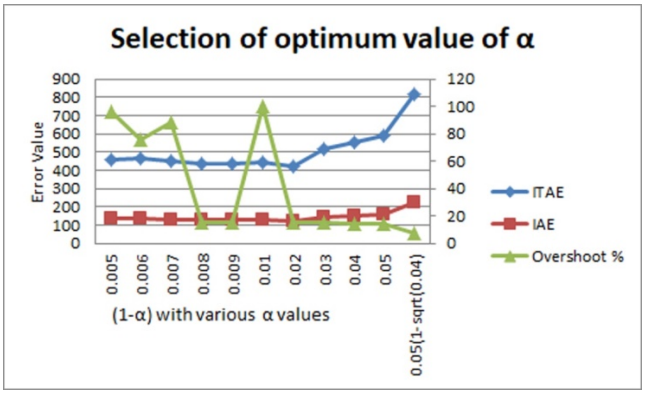


It is found that the optimal value of $\alpha$ for the SPW-ILC has been obtained as 0.04 with respect to the DC voltage rise time, reduced overshoot and integral time squared error (ITSE) and $\beta$ value as 0.05. By the introduction of $\beta$, overshoot in the $V_{dc}$ has been considerably reduced. The proposed HMG has been tested with various $\alpha$ values and with modified ILC; from Figure 7, it has been shown that the overshoot has been reduced with SPW-ILC, though error has been increased. In addition to that, the objective of maintaining the frequency and voltage within the limits has been achieved. And also, the smooth transition between the grid connected and autonomous mode of operation with the coordinated control of the sources, storage devices and loads could be achieved. Here after, the simulation and analysis of the proposed HMG has been done with the SPW-ILC.

Here after, the set point weighting factor ILC with forgetting factor has been considered and implemented.

## 4 Implementation of ILC in HMG

In this paper, the SPW-ILC for microgrid application has been proposed for enhancing the voltage and frequency in both grid connected and autonomous mode of operation. Figure 8 shows the implementation of ILC for microgrid operation.

**Figure 8** Implementation of ILC for interlinking converter (see online version for colours)

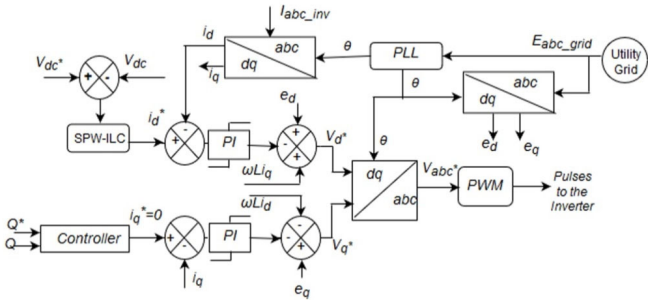


### *4.1 Autonomous mode of operation*

In standalone or autonomous mode of operation, the power from DGs' is fed to the DC bus. The bidirectional converter changes DC voltage into AC voltage maintained constant at AC bus. In order to maintain constant AC voltage at load side, the voltage at DC link is being compared with the reference voltage and the error is given to the Hybrid ILC. The system equations in dq reference frame can be written as:

$$e_{dg} = R_g i_{dg} + L_g \frac{di_{dg}}{dt} - \omega_g L_g i_{qg} + \vartheta_{dg} \tag{30}$$

$$e_{qg} = R_g i_{qg} + L_g \frac{di_{qg}}{dt} + \omega_g L_g i_{dg} + \vartheta_{qg} \tag{31}$$

$$\frac{di_{dg}}{dt} = -\frac{R_g}{L_g} i_{dg} + \omega_g i_{qg} - \frac{\vartheta_{dg}}{L_g} + \frac{e_{dg}}{L_g} \tag{32}$$

$$\frac{di_{qg}}{dt} = -\frac{R_g}{L_g} i_{qg} - \omega_g i_{dg} - \frac{\vartheta_{qg}}{L_g} + \frac{e_{qg}}{L_g} \tag{33}$$

$$\frac{d}{dt}\begin{bmatrix} i_{dg} \\ i_{qg} \end{bmatrix} = \begin{bmatrix} -\frac{R_g}{L_g} & \omega_g \\ \omega_g & -\frac{R_g}{L_g} \end{bmatrix} \begin{bmatrix} i_{dg} \\ i_{qg} \end{bmatrix} + \frac{1}{L_g}\left\{ \begin{bmatrix} e_{dg} \\ e_{qg} \end{bmatrix} - \begin{bmatrix} \vartheta_{dg} \\ \vartheta_{qg} \end{bmatrix} \right\} \tag{34}$$

where $\omega_g$ the angular frequency of the gird is, $\theta = \omega_g t + \theta_0$ is the synchronous rotating angle, $\theta_0$ is the initial value.

### 4.1.1 Outer voltage control loop

For the outer DC link voltage control loop, the $d$ axis reference grid current can be framed as

$$i_{dg}^{*} = (v_{dc}^{*} - v_{dc})(Gain\ of\ Ptype\ ILC) \tag{35}$$

Since the voltage control has been considered as the main objective, the reactive power control will be redundant in this case. Hence the q axis reference current has taken as zero.

$$i_{qg}^{*} = 0 \tag{36}$$

### 4.1.2 Inner current control loop

For the independent control of d-q axis grid currents, the cross couplings due to the coupling inductor are decoupled and the control signals are written as:

$$u_{dg}^{*} = -v_{dg} + \omega_g L_g i_{qg} + e_{dg} \tag{37}$$

$$u_{qg}^{*} = -v_{qg} - \omega_g L_g i_{qg} + e_{qg} \tag{38}$$

From the inner current control loop, the control signals are

$$u_{dg}^{*} = k_p \left( \frac{1 + pT_i}{pT_i} \right) (i_{dg}^{*} - i_{dg}) \tag{39}$$

$$u_{qg}^{*} = k_p \left( \frac{1 + pT_i}{pT_i} \right) (i_{qg}^{*} - i_{qg}) \tag{40}$$

Hence the decoupled d-q axes reference voltages for the grid side converter can be written as:

$$v_{dg}^{*} = -u_{dg}^{*} + \omega_g L_g i_{qg} + e_{dg} \tag{41}$$

$$v_{qg}^{*} = -u_{qg}^{*} + \omega_g L_g i_{dg} + e_{qg} \tag{42}$$

Substituting the $u_{dg}^{*}$ and $u_{qg}^{*}$ values in the above equation, the state space model of d-q axis reference voltages are

$$\begin{bmatrix} v_{dg}^{*} \\ v_{qg}^{*} \end{bmatrix} = \begin{bmatrix} -k_p & -\omega_g L_g \\ -\omega_g L_g & -k_p \end{bmatrix} \begin{bmatrix} i_{dg} \\ i_{qg} \end{bmatrix} + \begin{bmatrix} k_p & 0 \\ 0 & k_p \end{bmatrix} \begin{bmatrix} i_{dg}^{*} \\ i_{qg}^{*} \end{bmatrix} + \begin{bmatrix} k_i & 0 \\ 0 & k_i \end{bmatrix} \begin{bmatrix} X_d \\ X_q \end{bmatrix} + \begin{bmatrix} e_{dg} \\ e_{qg} \end{bmatrix} \tag{43}$$

where

$$\frac{dX_d}{dt} = i_d^{*} - i_d ; \frac{dX_q}{dt} = i_q^{*} - i_q$$

Using inverse park transformation, the abc reference voltages for the PWM modulator has been obtained as:

$$\begin{bmatrix} v_a^{*} \\ v_b^{*} \\ v_c^{*} \end{bmatrix} = \sqrt{2/3} \begin{bmatrix} \cos\theta & -\sin\theta & \sqrt{1/2} \\ \cos(\theta - 2\pi/3) & -\sin(\theta - 2\pi/3) & \sqrt{1/2} \\ \cos(\theta + 2\pi/3) & -\sin(\theta + 2\pi/3) & \sqrt{1/2} \end{bmatrix} \begin{bmatrix} v_d^{*} \\ v_q^{*} \\ 0 \end{bmatrix} \tag{44}$$

In this mode, the feed forward operation of the ILC control has been obtained as shown in Figure 9.

**Figure 9** Interlinking converter as inverter in autonomous mode of operation (see online version for colours)

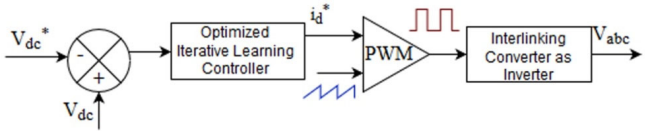


### 4.2 Grid connected mode of operation

In grid connected mode of operation, the hybrid ILC is producing the actual dc link voltage in the rectifier operation. The power has fed into AC bus from Grid in this mode. Through bidirectional converter, the power has been supplied to DC bus and charging the battery and meeting the DC loads. The feedback diagram has been demonstrated in Figure 10.

**Figure 10** Interlinking converter as rectifier in grid connected mode of operation (see online version for colours)

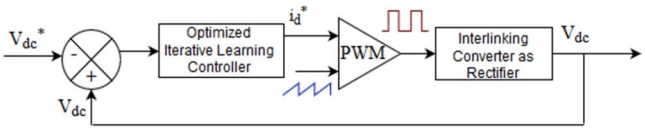


In this work, a novel method of SQP optimised ILC is implemented in hybrid AC/DC microgrid operation in both autonomous and grid-connected modes of operation.

## 5 Optimally tuned ILC by SQP

The bidirectional converter has a significant role in the proposed hybrid AC/DC microgrid operation, mostly when the microgrid is disconnected from the utility grid. Appropriate power management and control are necessary for the bidirectional converter to cope with the power flow from one sub-grid to another one. Power management of bidirectional converter control is predicted to manage the bidirectional power flow concerning both sub-grids. Hybrid AC/DC microgrid may perhaps be functioned in grid-connected and standalone mode. In grid-connected mode, the microgrid is linked through utility grid. To control AC system frequency in addition to voltage magnitude, utility grid supports a portion of power, even

though the DC sub-grid voltage is controlled through the bidirectional converter and BESS. In the event of systems containing DC sources connected with the DC bus, power will be supplied.

The primary objective of the proposed controller is to control the voltage variation in AC and DC buses even under the variations in the source and load. The power flow between the AC and DC bus is controlled by adjusting the voltage variation at the DC bus. The frequency and voltage of the AC bus is fixed due to its upstream network connection. So, the power balance in the AC sub-grid is affected by the control of HMG. Hence, proper control scheme is essential to control the DC voltage and to maintain the power balance in the DC sub-grid. Therefore, some controllers are essential for converter-based modules (i.e., bidirectional converter, BESS) for tracking the commands of controller in the device-level.

The operation of the BESS is controlled by the bidirectional buck-boost converter. For connecting the DC power sources to DC bus and to extract maximum power a unidirectional boost controller is utilised. A three-phase bidirectional converter connects DC sub-grid to AC sub-grid. In the proposed system, the microgrid's bidirectional converter and battery have the capability to control the DC bus voltage. Suppose, the battery SOC is between the $SOC_{min}$ and $SOC_{max}$, then the inverter works in constant power mode, which is programmed in the system-level optimisation. Consequently, for regulating the DC bus voltage, the supply any transient power shortage or absorb the extra-generated power in the DC sub-grid. Though, if the battery SOC extends its limits, the inverter will switch DC sub-grid voltage. The transient variation of DC voltage is given in the following equation (45).

$$V_{DC}(t) = \frac{1}{C}\int i_{total}\,dt + V_{DC}(t_0) \tag{45}$$

where $C$ is the capacitor at $DC$ bus. It can be modified as in (46):

$$V_{DC}(t) - V_{DC}(t_0) = \frac{1}{C}\int i_{total}\,dt \tag{46}$$

The net power balance extracted from total DC-link current and DC-link voltage is given in (47):

$$i_{total}(t) = \frac{1}{V_{DC}(t)}\begin{Bmatrix} P_{PV}(t) + P_{WT}(t) + \begin{bmatrix} P_{discharge}(t) \\ -P_{charge}(t) \end{bmatrix} \\ +P\left[\begin{pmatrix} P_{AC/DC}(t) * \eta_{AC/DC}(t) \\ -P_{DC/AC}(t) \end{pmatrix}\right] \\ -Load_{AC/DC}(t) \end{Bmatrix} \tag{47}$$

by substituting (47) in (46), the DC power balance equation attained based on DC-link voltage is given in (48):

$$V_{DC}(t) - V_{DC}(t_0) = \frac{1}{C.V_{DC}(t)}\begin{Bmatrix} P_{PV}(t) + P_{WT} \\ +\begin{bmatrix} P_{discharge}(t) \\ -P_{charge}(t) \end{bmatrix} \\ +P\left[\begin{pmatrix} P_{AC/DC}(t) \\ *\eta_{AC/DC}(t) \end{pmatrix}\right] \\ -P_{DC/AC}(t) \\ -Load_{AC/DC}(t) \end{Bmatrix} \tag{48}$$

As stated before, the power generated from solar and wind power systems are considered as uncontrollable generators, and they generate active power as much as possible. Therefore, if any power disturbance is occurred then that will be settled down by the battery and inverter. In the proposed system, an SQP optimised ILC controller is utilised to regulate the DC voltage and inject required current to maintain the power balance in DC sub grid. The SQP technique creates steps by solving quadratic sub problems. SQP is suitable for small and large problems and it is more suitable for solving problems with substantial nonlinearities. Initially, the grid voltage is measured and by using Park's transformation it is transformed into a synchronous $d - q$ reference frame for determining the inverter reference current. In the synchronous reference frame, the inverter power equations are given in (49) and (50):

$$P = \frac{3}{2}\left(V_d i_d + V_q i_q\right) \tag{49}$$

$$Q = \frac{3}{2}\left(V_q i_d - V_d i_q\right) \tag{50}$$

If the reference frame is concerned with beside a grid voltage, $V_q$ will be equivalent to zero. Formerly, by adjusting the direct in addition to quadrature current components the active as well as reactive powers are controlled. When battery SOC is between the $SOC_{min}$ and $SOC_{max}$, the current reference for controlling active power and reactive power in the d-axis and q-axis is given in (51) and (52):

$$i_d^* = \frac{3}{3V_d}P^* \tag{51}$$

$$i_q^* = \frac{2}{3V_d}Q* \tag{52}$$

where $P$* – reference active power (specified by level 1 controller), $Q$* – reference reactive power (set to zero). When DC bus voltage is controlled by the inverter, $i_q^*$ is set based on (51) and $i_d^*$ is set based on the voltage controller in the DC bus. Furthermore, to improve the power factor of the grid injected current, the requisite reactive power of AC load connected on AC bus will be compensated by the inverter.

In the proposed system, the parameters of the ILC are optimised by SQP technique. The general fact is to change the issue into the simpler sub-problem that would then be able to be settled and utilised as the premise of an iterative procedure. SQP is a nonlinear programming technique that intently imitates Newton's strategy for constrained optimisation similarly as is improved in the situation unconstrained optimisation. It begins from a solitary seeking point and finds a solution by utilising the gradient data, and depends on iterative formulation and the solution of a QP sub-problem.

The steps for the proposed SQP technique for ILC optimisation is followed as

*Step 1* Assign initial data: $x_0$, $\pi_0 > 0$, $\pi_b > 0$, $\rho > 0$, $\tau \in (0, 1)$ and $\sigma \in (0, 1)$.

For $k = 1, 2, \ldots$ up to the nonlinear program conditions are satisfied.

*Step 2* Define a positive definite matrix $B_k$ and compute the step $e^{iq}{}_k$ and multipliers $\lambda_{k+1}{}^{IQ}$, $\mu^{IQ}{}_{k+1}$ by solving the sub-problem.

*Step 3* Define the operational set $W_k$.

*Step 4* Compute the SQP step $e_k{}^{EQ}$ $k$ and multipliers $\lambda^{EQ}{}_{k+1,}$ $\mu^{EQ}{}_{k+1}$ by finding an approximate solution of the problem.

*Step 5* Compute the biggest number $\beta \in [0, 1]$ that confirms that the step $e = e^{IQ}{}_k + \beta\, d_{k+1}{}^{EQ}$ fulfils the restraints.

*Step 6* Compute the penalty parameter $\pi_k$.

*Step 7* Compute the step length $\alpha_k$, define $e_k$ by and set $X_{k+1} = x_k + d_k$.

*Step 8* Set $\lambda_{k+1} = \lambda_{k+1}{}^{EQ}$, $[\mu_{k+1}]W_k = \max(0, \mu^{EQ}{}_{k+1),}$ $[\mu_{k+1}]W_k{}^c = 0$.

Step 9 Find the best fit value.

In the proposed control scheme, instead of utilising the terminal voltage of each source, the voltage of common ac and dc buses are utilised. This scheme not only supplies precise power sharing but also outcomes in lesser voltage drop in common buses mostly in severely loaded conditions.

## 6 Results and discussion

The performance of the proposed HMG is evaluated using MATLAB/SIMULINK. A hybrid AC/DC microgrid is designed with solar power system, wind power system and BESS. In this proposed system, a DC microgrid is designed with a 7kW PV system and BESS. The PV system output power is controlled using a DC-DC converter. Additionally, a BESS is employed to store/supply power when the load demand is low/high. A 3 kW wind power conversion system is connected and considered as AC microgrid. Table.1 demonstrates the system specifications of the suggested system.

Permanent magnet synchronous generator (PMSG) based wind power system is simulated, and the output of this system is controlled by an AC-DC-AC converter. These ac and dc microgrids are interlinked with the bidirectional converter. Then this system is connected with AC loads, DC loads and the utility grid. The proposed system is tested with various conditions.

**Table 1** System specifications

| *System parameters* | *Values* |
|---|---|
| Solar system | Rated capacity= 7 kW |
| | Open circuit voltage = 406 V |
| | Maximum peak voltage = 336 V |
| | Shunt resistance = 550 Ω |
| | Series resistance = 0.055 Ω |
| Wind power system | Rated capacity= 3 kW |
| | Stator resistance = 0.0918 Ω |
| | Number of pole pairs = 4 |
| BESS | Nominal voltage = 400V |
| | Rated capacity = 6.5 Ah |
| Rated DC bus voltage | 415 V |
| Rated AC bus line voltage | 415 V |
| System frequency | 50 Hz |
| Capacitor across DC link | 1,200 μF |
| Loads | Resistive load = 20 KW |
| | Inductive load = 2 kVAR |

### *6.1 Simulation analysis*

The developed HMG is operated in grid-connected mode, the standalone mode under both variations in load and source conditions. Variation in source is achieved by varying solar irradiation and wind velocity. Table 2 explains the time duration of operating modes of the developed HMG system and its available connected sources and loads.

#### *6.1.1 Grid connected mode*

In this mode, the system operates for 0–3s. Among these, the resistive load of 20kW is connected to the system for 2.6s and resistive-inductive load is connected form 2.6–3s. In addition to these variations, input sources such as solar irradiation have been included for the study. At time t = 1 s, the irradiance of the solar system is reduced from 1,000 W/m$^2$ to 800 W/m$^2$. Therefore, the power produced by the PV system is reduced. To match this power, the grid will supply the required power to maintain the system reliability. At t = 1.4s, again the irradiance varies from 800 W/m$^2$ to 1,000 W/m$^2$. Then at t = 2s, an addition of 4.5 kW load is added with the help of the circuit breaker. By using the proposed coordinated controller, the additional required power is supply by the grid. In the grid-connected operation the battery is in charging mode. The reactive power produced by the PV and battery is always zero. At time t = 2.6s, an addition of 2 kVAR inductive load is connected.

Due to this, the reactive power at the load side is increased. To compensate this reactive power variation, grid supplies the required reactive power by tracking the $I_q$ value with $I_{q,ref}$.

**Table 2** Mode of operation with loads and the connected sources

| *Mode of operation* | *Simulation time (Secs)* | *Resistive-load (kW)* | *Inductive-load (kVAR)* | *Sources* |
|---|---|---|---|---|
| Grid connected Mode | 0.0–2 | 20 | - | G + PV + Wind |
| | 2–2.5 | 20 + 4.5 | - | G + PV + Wind |
| | 2.5–2.6 | 20 | - | G + PV + Wind |
| | 2.6–3 | 20 | 2 | G + PV + Wind |
| | 5–5.2 | 20 | - | G + PV + Wind |
| | 5.2–5.4 | 20 | - | G + Wind |
| | 5.4–6 | 20 | - | G + PV + Wind |
| Standalone mode | 3–3.8 | 9 | - | PV + Wind + Battery |
| | 3.8–4.3 | 9 + 2 | - | PV + Wind + Battery |
| | 4.3–4.7 | 9 | 4 | PV + Wind + Battery |
| | 4.7–5 | 9 | - | PV + Wind + Battery |
| | 6–6.5 | 9 | - | PV + Battery |
| | 6.5–7 | 9 | | PV + Wind + Battery |

### 6.1.2 Standalone mode

At t = 3s, the grid is disconnected, and now the hybrid AC/DC microgrid is operated under standalone mode. The power management is performed by the BESS during this mode. The load is decreased to 9 kW, and the PV system also generated only 5 kW power due to the reduction in its irradiance from 1,000 W/m$^2$ to 700 W/m$^2$. During this condition, the Wind power system generates 1 kW power, because of the decrement in the wind speed from 15m/s to 10 m/s. In order to compensate the power the BESS supplied the required 2 kW power. Up to t = 3s, the battery is in charging mode due to the grid connected mode of operation. When the operation is changed to standalone mode at t = 3s, the battery is in discharging mode, because, the BESS is started to supply the power.

At t = 3.4s, the irradiance of the solar system is increased to 800 W/m$^2$ and produces 6 kW power. Therefore, for managing the power, the power provided by the BESS is reduced from 2 kW to 1 kW. Similarly, at t = 3.8s, the load is increased to 11 kW, and the required power is supplied by the BESS. At the time the load is decreased to 5 kW, the PV system is sufficient enough to provide the required power. At this moment, the excess power generates by the wind power system is stored in the battery. At t = 4.3s, an inductive load of 4 kVAR is added, and the required reactive power is supplied by the controller from the capacitor which is connected at the dc-terminal of the bidirectional converter. It is understand that the bidirectional converter tracks the voltage reference which generates the required pulse signals for the converter to meet the required power demand.

### 6.1.3 Fluctuation of grid connected/ standalone mode for short

Figure11 shows the power output of the proposed system during grid connected and standalone mode of operations. From time t = 0–3s, the system is operated in grid-connected and t = 3–5s, the system is operated in standalone mode. Three phase breaker is used to connect and disconnect the grid with the microgrid. After the standalone mode operation, at time t = 5s, again grid is connected with the system and the power demand is controlled by the utility grid. At time t = 5.2 to 5.4 s, the PV system is completely disconnected by the breaker, because solar irradiation is not available in the night times. At that time, the grid will supply the required amount of power. Likewise, at time t = 6 to 7s, grid is disconnected, and the system is operated on a standalone mode of operation. At time t = 6 to 6.5 s, the wind power system is disconnected, and the load is also reduced from 20 kW to 9 kW. Since there is no grid power available, the battery system supplied the required 2 kW power.

**Figure 11** Coordinated control with proposed methodology (see online version for colours)

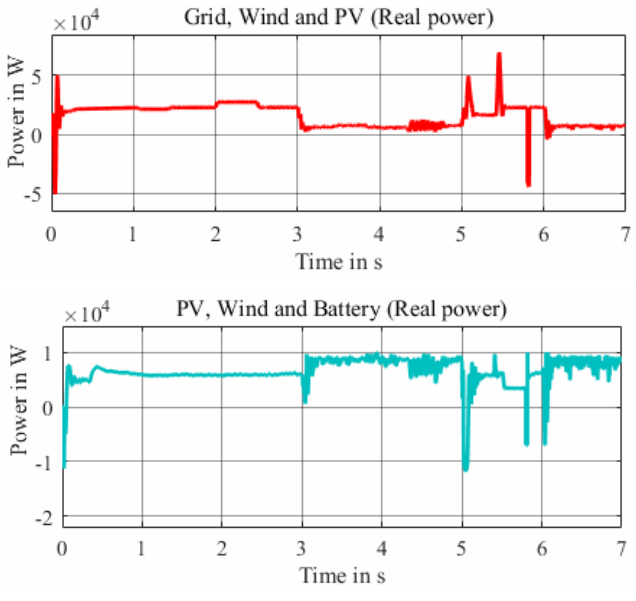

**Figure 11** Coordinated control with proposed methodology (continued) (see online version for colours)

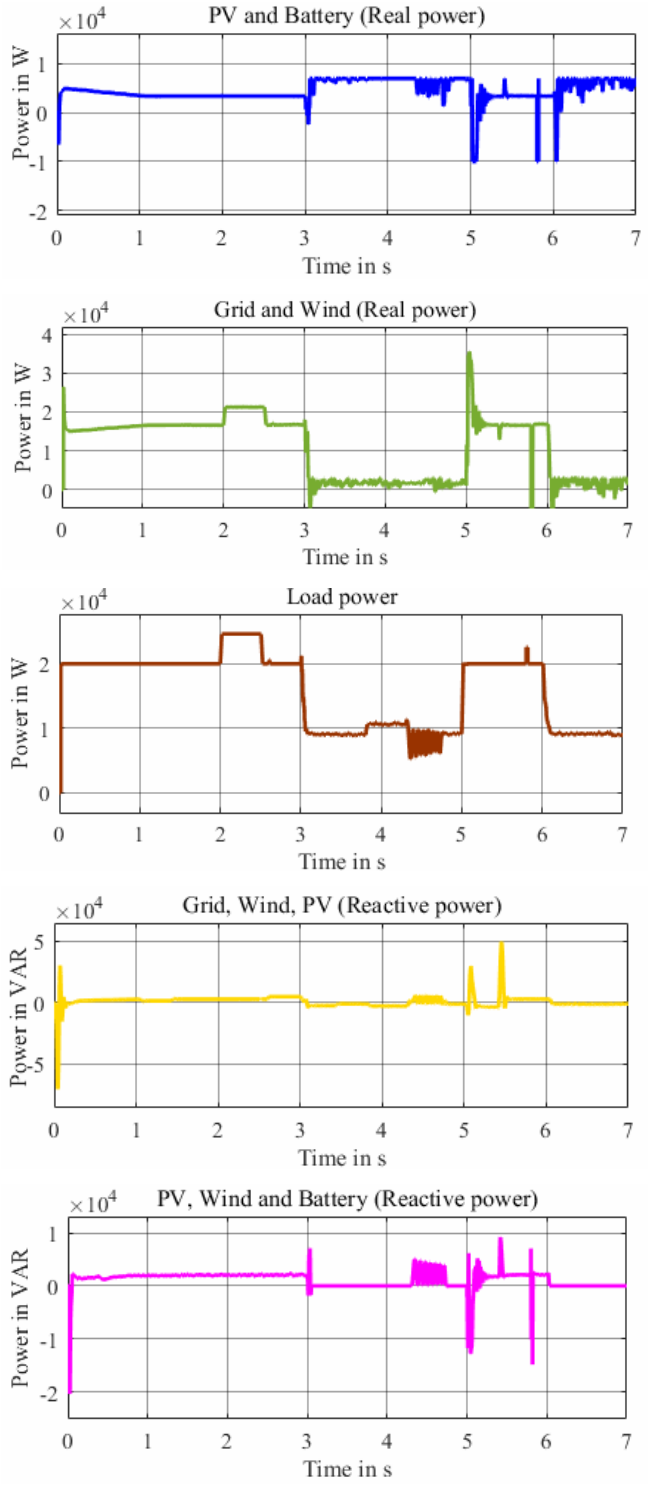


### 6.1.4 *Evaluation of controller performance*

To validate the performance of the controller, the proposed system is tested with conventional ILC and proposed SPW-ILC condition as shown in Figure 12. Generally, in the conventional microgrid configuration proportional integral (PI) controllers are employed to control the power flow. However, during the transition from grid-connected mode to standalone mode, variation in source and load conditions, the tracking efficiency of PI controllers are low. This will lead to oscillations in power as well as in the reduction in the reliability of the system. In Figure 12 at t = 3s, the system mode is changed from the grid-connected mode and at t = 5s, grid is again connected. During these transitions, proposed SQP optimised ILC controller efficiently tracked the changes in the load and source variations and provided better voltage support at the DC bus compared with the conventional ILC.

**Figure 12** DC Link voltage with conventional ILC and with SPW-ILC (see online version for colours)

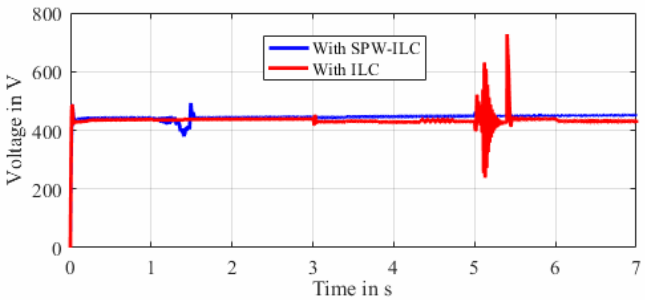


**Figure 13** Battery state of charge in all the modes (see online version for colours)

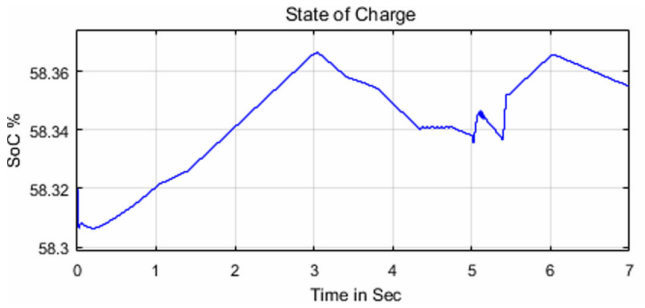


**Table 3** Performance Indices of various controllers for HMG system

| *Performance indices* | *Optimised ZN (PI)* | *Conventional ILC* | *SPW-ILC* | *SQP optimised SPW-ILC* |
|---|---|---|---|---|
| ITAE | 5583 | 5448 | 1043 | 796.6 |
| ITSE | $1.28*10^6$ | $1.27*10^6$ | $4.88*10^4$ | $2.628*10^4$ |
| Controller execution time (s) | 11.29 | 9.87 | 7.53 | 5.86 |
| Rise time (ms) | 70.99 | 65.36 | 11.434 | 11.485 |
| Percentage variation of DC link voltage | 97.35 | 96.492 | 11.65 | 11.30 |

The battery state of charge is shown in Figure 13. During grid connected mode, the battery is charging and in autonomous mode, it is discharging depending on the load value. The system operated without ILC cannot track this dynamic change and results in error in the power output.

This will affect the reliability of the overall hybrid AC/DC microgrid operation. But, with the proposed SQP optimised ILC, the bidirectional converter effectively tracks the load and source variation and the mode transitions too. This ensures the reliability of the hybrid AC/DC microgrid system.

Table 3 shows the comparison of SQP with Ziegler Nichols method (PI-control) and conventional ILC controller in terms of Performance indices such as integral time absolute error (ITAE), integral time square error (ITSE), controller execution time etc.

From Table 3, it is proved that, the proposed SQP optimised ILC controller is more reliable compared with the existing PI and ILC controller. The proposed controller has less execution time, rise time, fall time, ITAE and ITSE than the PI controller and providing better reliability in the hybrid AC/DC microgrid.

## 7 Conclusions

In this paper, a SQP technique based ILC is proposed to improve the reliability of the hybrid AC/DC microgrid. The system is tested with both grid connected and standalone mode operations. The simulation results showed that the proposed SQP optimised ILC Controller maintained the constant dc bus voltage irrespective of the variation in source and load condition which ensures more reliable HMG system. Furthermore, the performance of the proposed system is validated by operating with and without optimised ILC. The results demonstrated that the proposed system is well suitable for providing reliability to the HMG. In the future, the performance of the proposed SQP optimised ILC will be tested in real-time environments.

## References


Allam, M.A., Hamad, A.A., Kazerani, M. and El-Saadany, E.F. (2018) 'A novel dynamic power routing scheme to maximize load ability of islanded hybrid AC/DC micro grids under unbalanced AC loading', *IEEE Transactions on Smart Grid*, Vol. 9, No. 6, pp.5798–5809.

Angalaeswari, S. and Jamuna, K. (2015) 'Optimal placement and sizing of real power supporting DG in radial distribution networks', *IEEE International WIE Conference on Electrical and Computer Engineering (WIECON-ECE)*, Dhaka, pp.342–345.

Arimoto, S., Naniwa, T. and Suzuki, H. (1990) 'Robustness of P-type learning control with a forgetting factor for robotic motions', *Proceedings of the 29th Conference on Decision and Control*, December.

Chuang, S.J., Hong, C.M. and Chen, C.H. (2016) 'Design of intelligent control for stabilization of micro grid system', *International Journal of Electrical Power & Energy Systems*, November, Vol. 82, pp.569–578.

Deihimi, M.H., Naghizadeh, R.A. and Meyabadi, A.F. (2016) 'Systematic derivation of parameters of one exponential model for photovoltaic modules using numerical information of data sheet', *Renewable Energy*, Vol. 87, Part 1, pp.676–685.

Deng, H., Oruganti, R. and Srinivasan, D. (2007) 'Analysis and design of iterative learning control strategies for UPS inverters'. *IEEE Transactions on Industrial Electronics*, Vol. 54, No. 3, pp.1739–1751.

Golsorkhi, M.S., Shafiee, Q., Lu, D.D. and Guerrero, J.M. (2017) 'A distributed control framework for integrated photovoltaic-battery-based islanded micro grids', *IEEE Transactions on Smart Grid*, Vol. 8, No. 6, pp.2837–2848.

Kim, Y., Carbonetto, P., Stephens, M. and Anitescu, M. (2018) 'A fast algorithm for maximum likelihood estimation of mixture proportions using sequential quadratic programming', *Journal of Computational and Graphical Statistics*, arXiv:1806.01412, Taylor & Francis.

Lai, J., Zhou, H., Lu, X., Yu, X. and Hu, W. (2016) 'Droop-based distributed cooperative control for micro grids with time-varying delays', *IEEE Transactions on Smart Grid*, Vol. 7, No. 4, pp.1775–1789.

Li, X., Guo, L., Li, Y., Guo, Z., Hong, C., Zhang, Y. and Wang, C. (2018) 'A unified control for the dc–ac interlinking converters in hybrid AC/DC micro grids', *IEEE Transactions on Smart Grid*, Vol. 9, No. 6, pp.6540–6553.

Liu, J., Hossain, M.J., Lu, J., Rafi, F.H. and Li, H. (2018) 'A hybrid AC/DC micro grid control system based on a virtual synchronous generator for smooth transient performances', *Electric Power Systems Research*, September, Vol. 162, pp.169–182.

Liu, J., Rahman, M.S., Lu, J. and Hossain, M.J. (2016) 'Performance investigation of hybrid AC/DC micro grids during mode transitions', *Australasian Universities Power Engineering Conference (AUPEC)*, Brisbane, QLD, pp.1–6.

Lu, X., Yu, X., Lai, J., Guerrero, J.M. and Zhou, H. (2017) 'Distributed secondary voltage and frequency control for islanded micro grids with uncertain communication links', *IEEE Transactions on Industrial Informatics*, Vol. 13, No. 2, pp.448–460.

Mahmud, N., Zahedi, A. and Mahmud, A. (2017) 'A cooperative operation of novel PV inverter control scheme and storage energy management system based on ANFIS for voltage regulation of grid-tied PV system', *IEEE Transactions on Industrial Informatics*, Vol. 13, No. 5, pp.2657–2668.

Marzband, M., Azarinejadian, F., Savaghebi, M. and Guerrero, J.M. (2017) 'An optimal energy management system for islanded micro grids based on multiperiod artificial bee colony combined with Markov chain', *IEEE Systems Journal*, Vol. 11, No. 3, pp.1712–1722.

Mengelkamp, E., Gärttner, J., Rock, K., Kessler, S., Orsini, L. and Weinhardt, C. (2018) 'Designing micro grid energy markets: a case study: the Brooklyn micro grid', *Applied Energy*, 15 January, Vol. 210, pp.870–880.

Moayedi, S. and Davoudi, A. (2016) 'Distributed tertiary control of DC micro grid clusters', *IEEE Transactions on Power Electronics*, Vol. 31, No. 2, pp.1717–1733.

Moradi, M.H. and Abedini, M. (2016) 'A novel method for optimal DG units capacity and location in Micro grids', *International Journal of Electrical power & Energy Systems*, February, Vol. 75, pp.236–244.

Morstyn, T., Savkin, A.V., Hredzak, B. and Agelidis, V.G. (2018) 'Multi-agent sliding mode control for state of charge balancing between battery energy storage systems distributed in a DC micro grid', *IEEE Transactions on Smart Grid*, Vol. 9, No. 5, pp.4735–4743.

Pavlos, S.G. (2009) *Spotlight on Modern Transformer Design*, Springer, New York, ISBN: 978-1-84882-666-3.

Sedaghati, R. and Shakarami, M.R. (2019) 'A novel control strategy and power management of hybrid PV/FC/SC/battery renewable power system-based grid-connected micro grid', *Sustainable Cities and Society*, January, Vol. 44, pp.830–843.

Sun, K., Wang, X., Li, Y.W., Nejabatkhah, F., Mei, Y. and Lu, X. (2017) 'Parallel operation of bidirectional interfacing converters in a hybrid AC/DC micro grid under unbalanced grid voltage conditions', *IEEE Transactions on Power Electronics*, Vol. 32, No. 3, pp.1872–1884.

Ufnalski, B. (2017) 'On the similarity and challenges of multiresonant and iterative learning current controllers for grid converters and why the disturbance feed forward matters', SENE, Poland.

Ufnalski, B., Galeckl, A., Kaszewski, A. and Grzesiak, L.M. (2018) 'On the similarity and challenges of multiresonant and iterative learning current controllers for grid converters and why the disturbance feed forward matters', *Przegląd Elektrotechniczny*, Vol. 94, No. 5, pp.38–46, DOI. 10.15199/48.2018.05.07.

Xia, Y., Peng, Y., Yang, P., Yu, M. and Wei, W. (2017) 'Distributed coordination control for multiple bidirectional power converters in a hybrid AC/DC micro grid', *IEEE Transactions on Power Electronics*, Vol. 32, No. 6, pp.4949–4959.

Yang, P., Xia, Y., Yu, M., Wei, W. and Peng, Y. (2018) 'A decentralized coordination control method for parallel bidirectional power converters in a hybrid AC–DC micro grid', *IEEE Transactions on Industrial Electronics*, Vol. 65, No. 8, pp.6217–6228.

Zeraati, M., Golshan, M.E. and Guerrero, J.M. (2018) 'Distributed control of battery energy storage systems for voltage regulation in distribution networks with high PV penetration', *IEEE Transactions on Smart Grid*, Vol. 9, No. 4, pp.3582–3593.

## Nomenclature

$I_{PV}$ – Output current from the solar cell, A

$I_{Ph}$ – Current produced by light on the cell, A

$I_o$ – Reverse saturation current of the diode, A

$q$ – Electron's charge ($1.60217646 \times 10^{-19}$ C)

$k$ – Boltzmann constant($1.3806503 \times 10^{-23}$ J/K)

$T$ – Temperature of junction surface (Kelvin)

$n$ – Diode ideality factor

$V_i$ – Voltage across the diode and resistor, V

$N_s$ – Cells coupled in series

$V_T$ – Thermal Voltage, V

$V_{PV}$ – Voltage across the solar cell, V

$R_S$ – Series resistance in the solar cell, Ω

$R_p$ – Shunt resistance in the solar cell, Ω

$E$ – Kinetic energy, J

$\rho_A$ – Air density, kg/m$^3$

$v$ – Speed of airflow, m/s

$V$ – Wind velocity, m/s

$A_T$ – The blade swept region, m$^2$

$P_m$ – Mechanical power, W

$SoC$ – State of Charge of the battery,%

$V_{oc}$ – Open circuit voltage of the battery, V

$e_a$ and $\underline{e_b}$ – Voltages across the capacitors in the battery circuit, V

$I_{tb}$ – Current through the battery, A

$R_a$, $R_b$ – Resistances in the battery circuit, Ω

$C_a$ – Polarisation capacitance, F

$C_b$ – Incipient capacitance, F

$Q_m$ – Maximum battery charge, Ah

$P_b$ – Power output from the battery, W

$u_i(z)$ – z transform of the command at the iteration i

$k$ – Learning gain

$Ø(z)$ – Controller transfer function

$e_i(z)$ – z transform of tracking error ($y_d - y_i$)

$y_d$ – Desired output

$y_i$ – Actual output

$K_{RC}$ – Controller gain

$\beta$ – Set point weighting factor

$P_{PV}(t)$ – Power from PV at time t, W

$P_{WT}$ – Power from wind at time t, W

$P_{discharge}(t)$, $Pcharge(t)$ – Discharging and charging powers from battery at time t, W

$P_{AC/DC}(t)$ – Power converted from AC to DC at time t, W

$\eta_{AC/DC}(t)$ – Efficiency of IC as rectifier at time t

$P_{DC/AC}(t)$ – Power converted from DC to AC at time t, W

$Load_{DC}(t)$ – Load at DC bus, W

$e_{d,g}$, $e_{g,g}$ – d-q axes grid side voltages, V

$R_g$, $L_g$ – Resistance and Inductance of the coupling AC inductor, Ω, H

$i_{d,g}$, $i_{g,g}$ – d-q axes actual grid side currents, A

$\vartheta_{d,g}$, $\vartheta_{g,g}$ – d-q axes grid side converter voltages, V

$\omega_g$ – Angular frequency of the gird, rad/sec

θ – Synchronous rotating angle, rad

$\theta_o$ – Initial value, rad.